



Originally published as:

Orlecka-Sikora, B., Papadimitriou, E. E., Kwiatek, G. (2009): A study of the interaction among mining-induced seismic events in the Legnica-Głogów Copper District, Poland. - *Acta Geophysica*, 57, 2, 413-434

DOI: 10.2478/s11600-008-0085-z

A study of the interaction among mining induced seismic events in the Legnica–Glogow Copper District, Poland

B. Orlecka–Sikora¹, E.E. Papadimitriou², G. Kwiatek³

¹Faculty of Geology Geophysics and Environmental Protection, AGH University of Science and Technology, al. Mickiewicza 30, 30–059 Kraków, Poland, e–mail: orlecka@geol.agh.edu.pl – corresponding author

²Department of Geophysics, University of Thessaloniki, GR54124 Thessaloniki, Greece, e–mail: ritsa@geo.auth.gr

³GeoForschungsZentrum Potsdam, Dept. 3.2 Deformation and Rheology, Telegrafenberg D427, 14473 Potsdam, Germany, e–mail: kwiatek@gfz-potsdam.de

Abstract

Seismic hazard assessment in mining areas is of paramount importance for the nearby built environment since local events, although of small or moderate magnitude, because their locations are just beneath and very superficial, they have caused serious damage and often loss of life, and on top of that they exhibit a very high occurrence rate. Based on the fact that this activity also exhibits time dependence, as has been shown by several authors previously, and that small stress perturbation can enhance or prohibit future occurrences, we have applied the Coulomb stress transfer technique to investigate interactions among seismic events induced by mining works in the Rudna Mine in the Legnica–Głogów Copper District in south–west Poland. The coseismic stress changes due to tremor occurrences are only a small component of the stress field in mining areas and are not capable of generating a future seismic event. But if the rock mass at the location of the next event is already close enough to failure they can move it into the failure regime. Therefore, we have examined the influence of the cumulative static stress changes due to previous events on the generation of subsequent ones. For this purpose we considered events with energy greater than 10^5 J with a known focal mechanism that occurred in the LGCD area during the time period 1993–1999. We then calculated Coulomb stress changes (Δ CFF) after the occurrence of each event inverting each time the derived stress field according to the faulting type of the next event in the sequence of seismic events. We assumed the state of stress before the first seismic event in the analyzed sequence to be zero and the time changes of stress were referred to this initial value. At each stage of our calculations we attempted to correlate the location of the seismic event with the calculated values of Δ CFF.

The results of this study indicate that in many cases strong mining tremors produce changes in the state of stress of a sufficient magnitude to influence subsequent events. The location of

over 60% of events is consistent with stress-enhanced areas where the values of positive ΔCFF were above 0.01 MPa. For most of the events located inside areas of a calculated negative ΔCFF , their modelled rupture zone was partially located inside stress enhanced, providing thus additional evidence for possible triggering at the nucleation point.

Key words: LGCD, Rudna Mine, induced seismicity, Coulomb stress changes

1. INTRODUCTION

The mining history in the Lower Silesia (LS) area in south-west Poland goes back to the second half of the 1930s. Currently, copper ore is exploited in the Legnica-Głogów Copper District (LGCD), located in LS, in three mines: namely Lubin, Polkowice-Sieroszowice and Rudna. The long lasting mining activity has caused perturbation of the stress field in the rock mass, resulting in intense seismic activity. The mine seismological networks record every year several thousands events of local magnitudes ranging from 0.4 to 4.5. Within a large set of induced seismic events, rockbursts are the most serious phenomena in mining operations. Although rockbursts in the Polish mines are only a small subset of seismic events, they cause much damage with severe casualties. In the period 1985–2006 (22 years), on average three rockbursts were triggered annually by tremors, which resulted in over 10 accidents and two fatalities (Kłeczek, 2007). In the LGCD, the seismic activity also occurs directly beneath urbanized and industrialized areas, thus causing very strong ground motions affecting the natural and built environment. The strongest events have caused peak ground accelerations of almost 2.0 m/s^2 (Lasocki, 2005).

McGarr and Simpson (1997) classified seismicity accompanying mining exploitation as “induced” seismicity, which is expected to occur in response to stress changes that are comparable to typical earthquake stress drops. The generation process of mining induced seismic events is complicated by various time-variable factors of both natural and anthropogenic origin. In some regions of Poland, induced seismicity is also affected by the local geological and tectonic conditions. Strong tremors are considered as a result of interaction between the mining, lithostatic and tectonic stresses (e.g. Marcak, 1985; Gibowicz, 1990). Studies of seismicity in Polish mines have confirmed that at least two types of seismic events are observed, those directly connected with mining works and those associated with the movement on major geological discontinuities (e.g. Kijko *et al.*, 1985, 1987; Idziak *et al.*, 1991; Gibowicz and Kijko, 1994; Gibowicz and Lasocki, 2001). These two types of seismicity result in complex and multimodal magnitude distribution (e.g. Lasocki, 2001).

Lasocki (1992a, b) proved that the series of seismic events from individual mining stopes are not Poissonian, but show a time-variability in the long term. Several authors have also provided the evidence for interrelations of mining seismic events in the form of the spatio-temporal clustering of seismicity (e.g. Trifu *et al.*, 1993; Gibowicz, 1997; Orlecka-Sikora and Lasocki, 2002). Kijko (1997)

in studying the interevent time of seismicity from one of the deep gold mines in South Africa observed a trigger effect indicating internal correlations in the earthquake occurrence process. Similar conclusions have been derived by Węglarczyk and Lasocki (2008) who applied the Hurst rescaled analysis to the interevent times of seismicity from LGCD in Poland. Studies of the spatio-temporal distribution of seismicity recorded in the Creighton Mine in Canada, carried out by Marsan *et al.* (1999), confirmed the existence of a stress diffusion mechanism and its influence on the stronger events occurrence. Gibowicz (2006) found that the occurrence of mining-induced seismic events is capable of increasing the probability of a second event. The author analyzed the seismicity from the Wujek and Ziemowit coal mines and two copper mines in LGCD, namely the Polkowice and Rudna, and observed seismic doublets and multiplets in magnitude range of 0.7–3.5. They also noticed the correlation between the dominant direction of the doublets' spatial distribution and the azimuths of the nodal planes of some events forming doublets.

In recent years many studies of temporal and spatial patterns of earthquake occurrence have concentrated on examining possible correlations between earthquakes and the role of stress transfer in this process. Chinnery (1963) observed that changes in the stress field produced by a shear failure appeared in an area larger than one fault length. Later studies have presented the stress changes influencing the space-time patterns of aftershocks (e.g. Das and Scholz, 1981; Stein and Lisowski, 1983). Nowadays, fault interaction is considered as an integral part of the seismic hazard assessment, and is often investigated by static stress transfer models at different spatial and time scales (e.g. Harris, 1998 and the references therein; Steacy *et al.*, 2005 and the references therein).

Static stress changes are calculated considering a seismic source as a dislocation imbedded in a half-space and are expressed in terms of the Coulomb failure function (CFF) (e.g. King *et al.*, 1994; King and Cocco, 2001). The advantage of using this approach is that besides that the absolute value of stress is not known, stress changes can be calculated on the basis of details of geometry and the slip direction of earthquake rupture. The stress changes affecting subsequent events are typically of the order of 0.01 MPa, which are a small fraction of the corresponding stress drop (e.g. Harris, 1998 and the references therein). Coulomb stress changes can adequately explain the occurrence patterns of both small and strong events, and have been used as a powerful tool for the assessment of future seismic hazard in certain areas. Relevant studies have shown that this method is more effective if in addition to the accumulated stress changes due to the coseismic slips only, the long term tectonic loading is taken into account thus determining the evolution of the stress field in time (e.g. Deng and Sykes, 1997; Papadimitriou and Sykes, 2001).

The obtained results in natural seismicity encouraged us to apply the Coulomb stress transfer technique to investigate interactions among seismic events induced by mining works. The coseismic stress change associated with a given tremor is only one small component of the stress field in mining areas and is not enough to generate another seismic event, as is also the case in strong earthquake

occurrence. Nevertheless, if the rock mass at the location of the next event is already close enough to failure the first tremor can trigger the second one by introducing a positive Coulomb stress change to move it into the failure regime. Therefore, calculation of the static stress changes and their association with the spatial pattern of future occurrences will greatly contribute to the assessment of a future seismic hazard in LGCD.

Aiming to examine the influence of the cumulative static stress changes due to previous events on the generation of the next ones, the spatio-temporal earthquake occurrence in the Rudna mine area in LGCD in Poland is investigated and at each stage of the calculations the future occurrences are correlated with the resulted stress field, each time inverted according to the faulting type of the next event whose triggering is inspected.

2. METHOD

The first step in the analysis of faults interaction by modeling the static stress transfer is the calculation of the stress field associated with a particular fault. Static displacements, strains and stresses are calculated by solving the elastostatic equation for a dislocation on an extended fault in an elastic, isotropic and homogeneous half-space (e.g. King and Cocco, 2001). The displacement field produced by a dislocation Δu_j across a surface Σ in a uniform elastic half-space is given by Volterra's formula (Steketee, 1958a, b):

$$u_i = \int_{\Sigma} \Delta u_j \left[\delta_{jk} \lambda \frac{\partial u_i^l}{\partial \xi_l} + \mu \left(\frac{\partial u_i^j}{\partial \xi_k} + \frac{\partial u_i^k}{\partial \xi_j} \right) \right] \nu_k dS, \quad (1)$$

where δ_{jk} is the Kronecker delta, λ and μ are the Lamé's constants, u_i^j is the i th component of displacement at (x_1, x_2, x_3) due to a point force of unit magnitude (x_1, x_2, x_3) in the j -direction and ν_k is the outward normal vector to Σ . Fault geometry, the slip distribution and the strain nuclei are necessary for the computation of the static displacement. Chinnery (1961, 1963) and Okada (1985, 1992) have derived analytical expressions for the static displacement and strain fields caused by a finite rectangular fault at the Earth's surface and at any depth. The stress tensor components are calculated from the strain e_{ij} according to Hooke's law for an isotropic medium:

$$s_{ij} = \frac{2\mu\nu}{1-2\nu} \delta_{ij} e_{kk} + 2\mu e_{ij}, \quad (2)$$

where ν is the Poisson ratio and δ_{ij} is the Kronecker delta.

The second step is the choice of criterion characterizing failure in rocks. Among various criteria the more widely used is the Coulomb failure criterion (Jaeger and Cook, 1979; Scholz, 1990), which quantifies the closeness of a fault to failure. This criterion has been used by a number of authors to

study the distribution of aftershocks after a large earthquake and to investigate static stress changes on other faults in its vicinity (e.g. Das and Scholz, 1981; Stein and Lisowski, 1983; Reasenber and Simpson, 1992; Stein *et al.*, 1992; Hudnut *et al.*, 1994; King *et al.*, 1994; Parsons *et al.*, 1999). According to the Coulomb criterion, failure occurs on a plane when the Coulomb stress σ_f exceeds a specific value:

$$\sigma_f = \tau + \mu(\sigma_n + p), \quad (3)$$

where τ is the shear stress on the failure plane, σ_n is the normal stress, p is the pore fluid pressure and μ is the coefficient of friction. Both σ_n and τ are calculated for a fault plane at the observation point from the stress tensor defined by equation (2). The difference in the sign of τ indicates whether the potential for a slip on the plane is right- or left-lateral. The coefficient of friction and the fluid pore pressure can be combined together as the apparent coefficient of friction, μ' . Then the Coulomb failure function (CFF) (3) can be rewritten as:

$$\sigma_f = \tau + \mu' \sigma_n, \quad (4)$$

The change in shear stress is positive for increasing shear stress in the direction of a relative slip on the observed fault, the normal stress is positive for increasing tensional normal stress. A positive value of CFF moves a fault toward failure, a negative value of CFF moves it away from failure.

In the next step, the cumulative changes in stress due to the consecutive seismic events in the analyzed time series are calculated. We assume the state of stress before the first seismic event in the analyzed sequence to be zero and the time changes of stress are referred to this arbitrary zero baseline. In our work we do not take into account the mining and lithostatic stress changes caused by mining works, assuming that the stress changes were caused only by a coseismic slip. We put certain coseismic displacements on ruptured planes and add the changes in the components of the stress tensor as they occurred in time. It should be noted that stress is a tensional quantity and thus lobes with positive and negative stress changes must be viewed in the context of a specific type of faulting.

3. DATA

The seismic network at the Rudna Mine is composed of 32 vertical Wilmore MK2 and MK3 seismometers recording ground velocity. The seismometers are located at the level of copper ore deposits (except for a few ones located in shafts), at depths ranging from 300 m down to 1000 m. The signals are transmitted in analogue form with FM modulation by standard cables used in mining up to a central recorder located on the ground surface. Thereupon, signals are digitized with a sampling frequency equal to 500 Hz and 14-bit resolution. The whole system works in a triggering mode, the frequency band is from 0.5 to 150Hz and the system dynamics is approximately equal to 70dB (Domański *et al.*, 2002). The seismic network records annually several thousands of mining-induced

seismic events with local magnitudes, M_L , ranging from 0.4 up to 4.5, with the completeness cutoff being about 1.2. These events are considered to be directly related to copper ore mining.

For the following analysis, we selected the subset of 217 events with $M_L \geq 2.0$ (seismic energy equal to 1.0×10^5 J) that were recorded between June 6, 1993 and August 27, 1999. Figure 1 depicts the study area, along with the seismic stations and the spatial distribution of the seismic events incorporated in our stress changes calculations. Table 1 gives information on the annual number of events above a certain magnitude (energy class).

[FIGURE 1 SOMEWHERE HERE]

[TABLE 1 SOMEWHERE HERE]

The events, located by the mine's staff, exhibit uncertainties in the epicentral coordinates of the order of ± 50 m, which are much smaller than the uncertainty in depth determination (Leśniak & Pszczoła, 2008). This is because of the location of seismometers mainly at the level of copper ore deposits. There, one can expect seismic P waves propagating almost horizontally along the geological layers. It causes the problems with a proper detection of the first arrivals by the primarily vertical sensors. As a consequence, the spatial distribution of seismic stations makes the whole seismic network nearly planar (except for stations located in shafts), what results in a worse quality of the vertical component of location (Kijko, 1982). However, most of events in LGCD area occur very close to the exploitation level, directly above it or in an anhydrite layer c.a. 60 m above (Wiejacz, 1991) what may be a constrain on sources' depth. The estimated depth of analyzed events ranged from 0.3 km down to 1.1 km and, because accurate depth determination is not feasible, we performed the following calculations with the depth finally fixed to 0.9 km for all events, which is representative for the study area.

Two independent procedures were applied to the analyzed subset of seismic events: the moment tensor inversion in time domain for the determination of the focal parameters and a spectral analysis for the calculation of source parameters (Domański and Gibowicz, 2008). The detailed focal mechanism solutions were provided by the Institute of Geophysics of the Polish Academy of Sciences. The moment tensor inversion was based on the work of Fitch *et al.* (1980) and the special software adjusted to the geological situation within mines. The input parameters were the amplitude and polarity information on the first P-wave displacement pulses. Fortunately, the waveform field in the LGCD area displays the domination of refracted waves in the first P-wave arrivals over the direct P-wave onsets, which are seen only at the closest distances (< 1000 m). We observed significant head waves refracted from the crystalline baseground located below the exploitation level and composed of igneous rocks (incidence angle $\sim 60^\circ$) and from anhydrite layer from above (incidence angle $\sim 115^\circ$). Both types of waves could be detected and used for improving the coverage of the focal sphere and the

quality of fault plane solutions. Haskell's source model was assumed (Haskell, 1953) which requires the rupture time to be calculated from the average first P-wave pulse durations. According to Wiejacz (1991), this form of seismic source is expected to be a good approximation to the real mining-induced data in the LGCD area. The deviatoric, pure shear and full moment tensor were calculated using the L1 norm as a measure of the misfit and the method of the Lagrange multipliers (Wiejacz, 1991) was used in seismic moment tensor inversion. The uncertainties of strike, dip and rake do not exceed 15°.

The analysis of unconstrained and decomposed moment tensors revealed that the type of process responsible for the mine tremor source nucleation is not uniform. The generalized source mechanism of the analyzed mining-induced seismic events contained about 15 per cent of the isotropic component ISO, about 15 per cent of the uniaxial compressional or extensional component CLVD and about 70 per cent of the shear component DC in the total moment tensor solution. Fig. 2 presents the histograms of the particular components contributed to the total seismic moment tensor solution of the analyzed seismic events. The participation of the shear components in the focal mechanism is the most significant, and the higher values of CLVD and/or ISO component may be predominantly attributed to the inaccuracy of vertical component of location and, partially, to the insufficient focal sphere coverage, as was pointed out by Wiejacz (1991), among others. Table 2 gives information on the fault plane solutions of the strongest events.

[TABLE 2 SOMEWHERE HERE]

[FIGURE 2 SOMEWHERE HERE]

Spectral analysis was performed for a source-receiver distance greater than 3 km to suppress the influence of the near field effects and the complexity of the wave field. The amplitude of waveforms was corrected due to the vertical component used. A numerical integration filter was applied to the ground velocity records to obtain the displacement waveforms. The selected parts of P- and S-phases were tapered using a 10% von Hann's window, then the FFT was applied to both the ground velocity and displacement waveforms. The correction for instrument response has not been applied due to the higher frequency content of the recorded signals. The spectra were corrected for attenuation using $Q_p=400$ and $Q_s=200$, which represent the typical values of the quality factor used in LGCD. Spectral parameters were estimated from P and S components of vertical seismometers assuming the Ω^{-2} of Brune's model (Brune 1970, 1971) and the methodology developed by Andrews (1986). The J and K integrals provided by Snoke (1987) were used to estimate seismic moment and corner frequency and were corrected for limited frequency band. For the seismic moment, we applied the correction for radiation pattern. Free surface, as well as site corrections was not used due to the downhole location of seismic sensors.

It is very well known that the estimates of the seismic source size are heavily model-dependent. However, the quasidynamic model of circular fault of Madariaga (1976) with $K_P=2.01$ and $K_S=1.32$ for P and S waves, respectively, provides reasonable results in adequate agreement with independent observations in mines (e.g. Gibowicz and Kijko, 1994 and the references therein). The calculated circular fault radius and the seismic moment for each of the analyzed events are also given in Table 2. Typically we obtained at least 20 estimates of source parameters from both P and S phases for each event. The spectra that generated the outliers were reconsidered/removed and finally the average values of source parameters were calculated. The error of magnitude and source radius estimation (i.e. standard deviation), required for stress changes calculations, equaled to ± 0.1 and ± 50 m, respectively.

4. STRESS CHANGES CALCULATIONS AND EARTHQUAKE OCCURRENCE

Stress changes calculations were performed by the use of the software Coulomb 3.0 (Toda *et al.*, 2005; Lin and Stein, 2004). As it has been mentioned above, the stress field is inverted each time according to the faulting type of the next event. There is, however, no adequate information for the selection of the actual fault plane between the two determined. Although some generally accepted criteria were taken into account (a smaller dip angle in the case of dip slip events, similarity in the orientation of nearby events, etc), this selection is not unambiguous. Although it would result in intrinsic uncertainty when correlating stress changes and events locations, if this correlation were to be proved significant then the expectedly stronger correlation for the set of actual nodal planes would be significant as well.

The geomechanical parameters of rocks in the LGCD vary in a wide range depending on the type of rocks (e.g. Piestrzyński, 1996). We performed calculations with the shear modulus and the Poisson ratio fixed as $2.2 \cdot 10^4$ MPa and 0.25, respectively, and the apparent coefficient of friction was taken to be equal to 0.8 throughout our calculations.

The circular fault radius and seismic moment were used to calculate two additional parameters necessary for the stress transfer model application, namely the fault dimension and average displacement. The values of the circular fault radius were recalculated to the length and width of the corresponding rectangular fault. The coseismic displacement along the ruptured plane was estimated from the seismic moment, by taking the shear modulus equal to $2.2 \cdot 10^4$ MPa and considering the fault area (e.g. Aki and Richards, 1980). Information on the rupture models of the events included in our calculations is given in Table 3.

[TABLE 3 SOMEWHERE HERE]

Fig. 3 presents histograms of the frequency of seismic tremor occurrence as a function of CFF changes (ΔCFF) due to previous occurrences. The first histogram presents the frequency of all the analyzed seismic events, while the second one only the events with a seismic moment larger or equal to 10^{13} [N·m]. Negative changes in Coulomb stress denote a decreased likelihood of fault rupture, while positive CFF changes denote an increased likelihood of failure. About 61 per cent of the total considered seismic tremors occurred at locations of positive changes in stress created by previous events. Most of these events, about 50 per cent, were located inside regions of ΔCFF values larger than 0.01 MPa. In the cases of stronger tremors, those with $M_0 \geq 10^{13}$ [N·m], the percentage of events occurred at locations with positive changes is almost the same and more particularly, equal to 63% of the total number of events. The remaining events occurred in areas of calculated negative ΔCFF but for most of them the modeled rectangular fault is located partially inside stress enhanced areas, although the hypocentre is located inside stress shadows (Fig. 4d, f). These observations provide evidence for their possible triggering considering the nucleation point being inside positive stress areas.

[FIGURE 3 SOMEWHERE HERE]

Fig. 4 shows snapshots of the cumulative stress changes in the study area at a depth of 0.9 km in the G-1/7 field of the Rudna Mine. The mine field is the unit of mine division, section of mine, the region with the part of copper ore deposit intended for the extraction by the determined exploitation method. The ΔCFF was calculated by taking into account all the events in our dataset, while in Figure 4 only the events that are marked to have occurred in G-1/7, are depicted. The white in Fig. 4 indicates no significant changes in Coulomb stress, blue regions denote negative changes and yellow to red regions represent positive CFF changes. The mining works in the G-1/7 field were carried out in the right bottom quadrant of pictures in a NW-SE direction.

[FIGURE 4 SOMEWHERE HERE]

Fig. 4a shows the cumulative Coulomb stress changes due to the first 76 tremors in the studied dataset, calculated according to the fault plane solution of the next event that occurred on 23.04.1996 in the G-1/7 field of the Rudna Mine. These events created in the G-1/7 field a shadow zone in a SW-NE direction and two bright zones in the north-western and south-eastern parts (Fig. 4a). The 23.04.1996 event occurred at the border between bright and shadow zones, making triggering by ΔCFF doubtful. Then 8 other tremors with magnitude from 2 to 2.6 occurred in the vicinity of G-1/7, 5 in bright zones and 3 in shadows.

Fig. 4b presents the state of the accumulated stress changes due to the first 85 seismic events in our data sample, calculated according to the faulting type of the next event. These events caused a large shadow zone in G-1/7 except for two smaller bright zones in the northern part of the area. The next event with local magnitude of 2.9 occurred on 07.11.1996 in one of these two stress-enhanced zones.

Fig. 4c presents the state of stress just before the occurrence of the 88th event occurring on 08.11.1996, inverted according to its faulting type. After the occurrence of the previous event, on 07.11.1996, a bright zone was created at the site of the 88th event thus providing evidence of its probable triggering; evidence that is more substantiated by the small difference in the occurrence time of the two events (just one day).

The cumulative Δ CFF were calculated for faulting in agreement with the focal plane solution of the next tremor, which occurred on 19.12.1996 (Fig. 4d). The epicenter of this event is located in a patch of the shadow zone but its rupture zone is partially located inside the bright zone. The partial location of the fault inside a stress enhanced area provides evidence of possible triggering.

After the 19.12.1996 event, 51 more tremors with $M_L \geq 2.0$ occurred in the Rudna mine, 21 of them in the vicinity of G-1/7. Fig. 4e shows the state of stress just before the 09.09.1998 event of $M_L 2.8$. Positive Δ CFF occupied a large zone in the western part of the area, continuing to the north-east and two smaller zones in the south-east. The epicenter of the 09.09.1998 tremor was located inside a bright zone, and more particularly at a site where the positive Δ CFF had a value equal to 0.26 MPa.

Fig. 4f presents the cumulative Coulomb stress changes associated with the sequence of events considered earlier and additionally, the next 20 occurred in the Rudna mine before 13.10.1998. The stress shadow is now limited to 3 zones, the first of them starting at the centre of the G-1/7 field and continues to the north, the second located to the east part of the study area, and the third at the southern part. The next event occurred on October the 13th 1998, with its epicenter being inside a shadow zone, while about 30% of its rupture area is located inside a stress-enhanced zone. One can observe that the large bright zones in the south-western and south-eastern part of G-1/7 still did not experience events. The explanation is that the seismic events are induced by mining works and events are expected to occur in places where exploitation is carried out.

The snapshot of Fig. 4g indicates the cumulative stress changes until just before the 04.07.1999 event. It includes the stress changes caused by 29 additional events which occurred during 9 months from the last 13.10.1998 event in the Rudna mine and 10 of them in surrounding fields of the G-1/7 area. The epicenter of the 04.07.1999 event is located in a small patch of negative Δ CFF, although the largest part of its rupture area is inside a stress enhanced area. Fig. 4h depicts the state of stress just after this event, calculated for the fault plane solution of the next 05.07.1999 event, ($M_L=2.9$), which is located at a place of positive Δ CFF equal to 0.03 MPa. The stress drop caused by this event is one order larger than the corresponding Δ CFF and equal 0.67MPa.

The addition of coseismic stress changes associated with the occurrence of the next inspected 5 events in the Rudna mine is shown in Fig. 4i. These events caused enlargement of the shadow zone in the north–eastern part of the presented area. The next event occurred on 12.08.1999 in a stress–enhanced zone, where the ΔCFF was as before, equal to 0.03 MPa.

The occurrence of the 12.08.1999 event caused the appearance of an additional stress shadow zone on the south–west (Fig. 4j). In the area where the exploitation was carried out the next event happened on 13.08.1999. The epicenter of this event is located at the border between a bright zone and a stress shadow.

5. CONCLUSIONS

We investigated possible interactions through perturbations of the stress field due to the coseismic slip of the mining induced seismic events that occurred in the Rudna mine in the Legnica–Głogów Copper District. For this purpose we modeled the static stress changes, represented by the Coulomb failure function, due to the sequence of 217 seismic events of local magnitudes ranging from 2.0 to 4.2, which occurred in this mine between June 6, 1993 and August 27, 1999. The coseismic displacements used in this study were simplified to be vectors across a rectangular fault in elastic half–space. We calculated Coulomb stress changes after the occurrence of each event according to the faulting type of the next event in the dataset. At each stage of calculations we examined the possible triggering effect by correlating the particular event location and the stress–enhanced zones. In the calculations we chose one of the nodal planes from the catalog at random, assuming that if a correlation between event locations and CFF changes is significant the expectedly stronger correlation for the set of actual nodal planes would be significant as well.

The results of our preliminary study indicate that strong mining tremors are capable of producing changes in the state of stress of a sufficient magnitude to move a specified area into the failure regime. We found that the location of more than 60% of the analyzed events is consistent with the stress–enhanced areas. Most of the events were located inside regions of positive ΔCFF , larger than 0.01 MPa. The remaining events were located inside areas of calculated negative ΔCFF but for most of them the modeled rupture zone was located partially inside areas of positive ΔCFF . Furthermore, more than 15 per cent of these events had a doubtful focal mechanism.

We presented the model of stress evolution in the G–1/7 section of the Rudna mine. Among the 10 events that occurred in the G–1/7 field between 23.04.1996 and 12.08.1999, 5 were located in stress–enhanced zones, 2 events were located at the border between the positive and negative stress changes. The epicenters of 3 events were located inside shadow zones, while the largest part of the rupture areas of 2 of them were well inside a bright zone. These results provide evidence of possible triggering due to stress transfer by previous events occurrence in the G–1/7 field. The modeling of stress changes due

to seismic events along with the progress of mining works can provide additional information for determining more probable zones for future tremor location.

There are several assumptions and uncertainties in our approach. The errors of event location in the LGCD are about ± 50 m for epicentral determination and much higher for depth. This last uncertainty led us to assume a nucleation depth equal to 900 m. The next group of parameters that have an impact on the results of analysis and are characterized by a wide range of possible values are the elastic moduli of rocks in the Rudna mine. The selected values reflect the averaged geomechanical conditions in LGCD, where the seismogenic zone is composed of limestones, dolomites, anhydrites and sandstones. The apparent coefficient of friction that was taken equal to be 0.8 throughout our calculations, is much higher than for Coulomb stress transfer modeling performed for natural earthquakes because rocks in the mining area are characterized by a higher cohesion than is the case in seismic fault zones. The proper determination of rupture plane (strike, dip and rake) from nodal planes provided by the fault plane solution plays a key role in Coulomb stress transfer studies. In our calculations, the choice of a particular fault plane depended on its similarity to the focal mechanisms of previous events that had occurred in the vicinity of the studied earthquake. In some sections of the mine the fault plane orientation parameters for seismic events are similar, indicating a common origin. If this information was not accessible, the fault plane was chosen randomly. We considered only events with rather reliably determined fault plane solutions. Therefore we had to assume that the state of stress before 06.1993 was zero.

Although a number of uncertainties are involved in the calculations, the results of the preliminary stress changes modeling in the Rudna mine in LGCD are promising, since it has been shown that most of the events occurred in areas where stress was enhanced due to the occurrence of previous events. For this reason, this approach can be incorporated in seismic hazard assessment studies. On the other hand, much work and detailed investigation should be carried out to prove the role of Coulomb stress transfer in the generation process of the mining induced seismicity.

A c k n o w l e d g e m e n t s . This work was prepared within the framework of the research project No. PBS–Grecja/10/2007, financed by the Ministry of Education and Science of Poland during the period 2007 to 2009. We thank S.J. Gibowicz, B.M. Domański and P. Wiejacz for sending us the unpublished catalog of focal mechanism solution and spectral analysis parameters for strong seismic events from Rudna Mine.

References

Aki, K. and P. Richards (1980), *Quantitative Seismology: Theory and Methods*, W.H. Freeman, San Francisco.

- Andrews, D. (1986), Objective determination of source parameters and similarity of earthquakes of different size, **In:** S. Das, Boatwright, J. and C. Scholz (ed.), *Earthquakes source mechanics*, **37**, 259–267.
- Brune, J. N. (1970), Tectonic stress and spectra of seismic shear waves from earthquakes, *J. Geophys. Res.* **78**, 4997–5009.
- Brune, J. N. (1971), Correction, *J. Geophys. Res.* **76**, 5002.
- Chinnery, M.A. (1961), The deformation of the ground around a surface fault, *Bull. Seism. Soc. Am.* **51**, 355–372.
- Chinnery, M. A. (1963), The state of stress changes that accompany strike-slip faulting, *Bull. Seism. Soc. Am.* **53**, 921–932.
- Das, S. and C.H. Scholz (1981), Theory of time-dependent rupture in the earth, *J. Geophys. Res.* **86B**, 6039–6051.
- Deng, J. and L. R. Sykes (1997) Evolution of the stress field in southern California and triggering of moderate-size earthquakes: a 200-year perspective, *J. Geophys. Res.* **102**, 9859–9886.
- Domański, B. and S.J. Gibowicz (2008), Comparison of source parameters estimated in the frequency and time domains for seismic events at Rudna copper mine, Poland, *Acta Geophys.* **56**, 324 – 343. DOI: 10.2478/s11600-008-0014-1.
- Domański, B., Gibowicz, S. J., Wiejacz, P. (2002), Source time function of seismic events at Rudna copper mine, Poland, *Pure Appl. Geophys.* **159**, 131–144.
- Fitch, T. J., McCowan, D. W., Shields, M. W. (1980), Estimation of seismic moment tensor from teleseismic body wave data with application to intraplate and mantle earthquakes, *J. Geophys. Res.* **85**, 3817–3828.
- Gibowicz, S.L. (1990), The mechanism of seismic events induced by mining. In: *Rockburst and seismicity in mines*, Rotterdam, Balkema, 3–27.
- Gibowicz, S.J. (1997), An anatomy of a seismic sequence in a deep gold mine, *Pure Appl. Geophys.* **150**, 393–414.
- Gibowicz, S.J. (2006), Seismic doublets and multiplets at the Polish coal and copper mines, *Acta Geophys.* **54**, 142-157. DOI 10.2478/s11600-006-0014-y.
- Gibowicz, S. J. and A. Kijko (1994) *An Introduction to Mining Seismology*, Academic Press, San Diego.
- Gibowicz, S.J. and S. Lasocki (2001), Seismicity induced by mining: Ten years later, *Advances in Geophysics*, **44**, 39–181.
- Harris, R. A. (1998) Introduction to special session: stress triggers, stress shadows, and implications for seismic hazard, *J. Geophys. Res.* **103**, 24347–24358.

- Haskell, N. A. (1953), The dispersion of surface waves in multilayered media, *Bull. Seismol. Soc. Am.*, **43**, 17–34.
- Harris, R. A. and R.W. Simpson (1996), In the shadow of 1857: the effect of the great Ft. Tejon earthquakes in southern California. *Geophys. Res. Lett.* **23**, 229–232.
- Hudnut, K. W., Y. Bock, M. Cline, P. Fang, Y. Feng, J. Freymueller, X. Ge, W. K. Gross, D. Jackson, M. Kim, N. E. King, J. Langbein, S. C. Larsen, M. Lisowski, Z. K. Shen, J. Svarc, Zhang, J. (1994), Co-seismic displacements of the 1992 Landers earthquake, *Bull. Seismol. Soc. Am.*, **84**, 625–645.
- Idziak, A., Sagan, G, Zuberek, W.M. (1991), The analysis of energy distribution of seismic events from the Upper Silesian Coal Basin, *Publ. Inst. Geophys. Pol. Acad. Sci.* **M–15 (235)**, 163–182, (in polish).
- Jaeger, J.C. and N.G.W. Cook (1979), *Fundamentals of rock mechanics* (3rd ed.), London, Chapman and Hall.
- Kijko, A. (1997), Keynote lecture: seismic hazard assessment in mines. **In:** S.J. Gibowicz and S. Lasocki (ed.), *Rockbursts and Seismicity in Mines*, Balkema, Rotterdam, 247–256.
- King G.C.P. and M. Cocco (2001), Fault Interaction By Elastic Stress Changes: New Clues From Earthquake Sequences. *Advance in Geophysics*, **44**, 1–38.
- Kijko, A., Drzeźła B., Mendecki, A. (1985), Why the extremal seismic events distribution have the bimodal character? *Acta Montana*, **71**, 225-244, (polish).
- Kijko, A., Drzeźła, B., Stankiwicz, T. (1987), Bimodal character of extreme seismic events in Polish mines, *Acta Geophys. Pol.* **35**, 157–166.
- Kijko, A., Dessokey, M. M., Głowacka, E., Kazimierczyk, M. (1982), Periodicity of strong mining tremors in the Lubin copper mine, *Acta Geophys. Pol.* **30**, 221–230.
- King, G, C. P., Stein, R. S., Lin, J. (1994), Static stress changes and the triggering of earthquakes, *Bull. Seismol. Soc. Am.*, **84**, 935–953.
- Kłeczek, Z. (2007), Sterowanie wstrząsami górotworu LGOM (Control of rock-mass bursts in Polish Copper Mines LGCD). **In:** *Warsztaty Górnicze 2007 „Zagrożenia naturalne w górnictwie”*, Ślesin k. Konina, 4–6 czerwca 2007 r. Bezp. Pr. Ochr. Śr. Gór. 2007 nr 6, 25–27.
- Lasocki, S. (1992a), Non-Poissonian structure of mining induced seismicity, *Acta Montana*, **84**, 51–58.
- Lasocki, S. (1992b), Weibull distribution for time intervals between mining tremors, *Publ. Inst. Geophys. Pol. Acad. Sci.* **M–16 (245)**, 241–260.
- Lasocki, S. (2001), Quantitative Evidences of Complexity of Magnitude Distribution in Mining-induced Seismicity: Implications for Hazard Evaluation. **In:** G. van Aswegen, R.J. Durrheim, W.D. Ortlepp (ed.), *5th Int. Symp. Rockbursts and Seismicity in Mines "Dynamic rock mass*

- response to mining*", Magalisberg, 17–20 September 2001 SAIMM S27, Johannesburg, South Africa, 543–550.
- Lasocki, S. (2005) Probabilistic Analysis of Seismic Hazard Posed by Mining Induced Events, In: Y. Potvin, M. Hudyma (ed.), *The Sixth International Symposium on Rockbursts and Seismicity in Mines "Controlling Seismic Risk" Proceedings*, ACG, Perth, 151–156.
- Leśniak, A., Pszczoła, G. (2008), Combined mine tremors source location and error evaluation in the Lubin Copper Mine (Poland), *Tectonophysics* **456**, 16-27.
- Lin, J. and R.S. Stein (2004), Stress triggering in thrust and subduction earthquakes, and stress interaction between the southern San Andreas and nearby thrust and strike–slip faults, *J. Geophys. Res.* **109**, B02303, doi:10.1029/2003JB002607.
- Madariaga, R. (1976), Dynamics of an expanding circular fault, *Bull. Seismol. Soc. Am.* **66**, 639–666.
- Marcak, H. (1985), Geophysical models of development of destruction process in the rock mass prior to rockburst. *Publ. Inst. Geophys. Pol. Sc. Acad.* **M–6 (176)**, 149–174, (in polish).
- Marsan, D., Bean, Ch.J., Steacy, S., McCloskey, J. (1999), Spatio-temporal analysis of stress diffusion in mining–induced seismicity system, *Geophys. Res. Lett.* **26**, 3697–3700.
- McGarr, A. and D. W. Simpson (1997), Keynote lecture: a broad look at induced seismicity, In: S. J. Gibowicz and S. Lasocki (ed.), *Rockbursts and Seismicity in Mines*, Balkema, Rotterdam, 385–396.
- Okada, Y. (1985), Surface deformation due to shear and tensile faults in a half-space. *Bull. Seism. Soc. Am.* **75**, 1135–1154.
- Okada, Y. (1992), Internal deformation due to shear and tensile faults in a half–space. *Bull. Seism. Soc. Am.* **82**, 1018–1040.
- Orlecka–Sikora, B. and S. Lasocki (2002), Clustered structure of seismicity from the Legnica–Głogów copper district, *Publ. Inst. Geophys. Pol. Acad. Sc.*, **M–24 (340)**, 105–119, (in polish).
- Papadimitriou, E. E., and L. R. Sykes (2001), Evolution of the stress field in the northern Aegean Sea (Greece), *Geophys. J. Int.* **146**, 747–759.
- Parsons, T., Stein, R. S., Simpson, R. W., Reasenber, P. A. (1999), Stress sensitivity of fault seismicity: a comparison between limited–offset oblique and major strike–slip faults, *J. Geophys. Res.* **104**, 20183–20202.
- Piestrzyński, A. (1996), *Monografia KGHM Polska Miedz SA. Centrum Badawczo-Projektowe Miedzi "Cuprum"*. Wrocław.
- Reasenber, P. A. and R. W. Simpson (1992), Response of regional seismicity to the static stress change produced by the Loma Prieta earthquake, *Science*, **255**, 1687-1690.

- Scholz, C.H. (1990), *The mechanics of earthquakes and faulting*, Cambridge, U.K., Cambridge University Press, 439.
- Snoke, J. A. (1987), Stable determination of (Brune) stress drops, *Bull. Seismol. Soc. Am.*, **77**, 530-538.
- Stacy S., Gomberg J., Cocco, M. (2005), Introduction to special section: stress transfer, earthquake triggering and time-dependent seismic hazard, *J. Geophys. Res.* **110**, doi:10.1029/2005JB003692.
- Stein, R. S. and M. Lisowski (1983), The 1979 Homestead Valley earthquake sequence, California: Control of aftershocks and postseismic deformation, *J. Geophys. Res.* **88**, 6477–6490.
- Stein, R.S., King, G.L.P., Lin, J. (1992), Change in failure stress on the southern San Andreas fault system caused by the 1992 magnitude=7.4 Landers earthquake, *Science*, **258**, 1328–1332.
- Steketee, J.A. (1958a), On Volterra's dislocations in a semi-infinite elastic medium. *Can. J. Phys.* **36**, 193–205.
- Steketee, J.A. (1958b), Some geophysical applications of the elasticity theory of dislocations. *Can. J. Phys.* **36**, 1168–1198.
- Toda, S., Stein, R. S., Richards-Dinger, K., Bozkurt, S. (2005), Forecasting the evolution of seismicity in southern California: Animations built on earthquake stress transfer, *J. Geophys. Res.* **B05S16**, doi:10.1029/2004JB003415.
- Trifu, C.-I., Urbancic, T.I., Young, R.P. (1993), Non-similar frequency-magnitude distribution for $M < 1$ seismicity, *Geophys. Res. Lett.* **20**, 427–430.
- Węglarczyk, S. and S. Lasocki (2008), Studies of long and short memory in mining-induced seismic processes, *Acta Geophysica* (submitted).
- Wiejacz, P. (1991), Investigation of focal mechanisms of mine tremors by the moment tensor inversion, Ph. D. Thesis, Inst. Geophys. Pol. Ac. Sci., Warsaw, Poland.

Table 1. Annual number of events per magnitude / energy class in the Legnica–Głogów Copper District in the years 06.1993–08.1999. M_L denotes the local magnitude, while energy (E) is expressed in joules.

Table 2. Source parameters of $M_L \geq 3.0$ mining induced seismic events that occurred between 08.1994 – 08.1999 in the Rudna mine area in the LGCD. The first three columns provide information on the occurrence date and time, X, Y, Z denote location in the local Cartesian coordinate system, M_L denotes the local magnitude, E energy, M_0 seismic moment, r is the circular fault radius. The last six columns provide information of the fault plane solution (strike, dip and rake for both nodal planes).

Table 3. Rupture models for mining induced seismic events with $M_L > 3.0$ that occurred between 08.1994 – 08.1999 in the Rudna mine area in the Legnica-Głogów Copper District, included in the Coulomb stress transfer calculations. L and W denote the length and width of the rectangular fault, respectively, expressed in meters, u is the mean displacement, ss, along strike and ds, along the dip direction, expressed in centimeters.

Table 1

Year	Number of seismic events					
	E [J]	10^5	10^6	10^7	10^8	10^9
	M_L	2	2.5	3	3.5	4
1993		0	1	0	0	0
1994		11	3	9	1	0
1995		34	11	4	2	0
1996		8	4	0	0	0
1997		9	9	10	0	0
1998		43	21	9	1	0
1999		17	6	2	1	1
Total		122	55	34	5	1

Table 2

Origin			Hypocentre			Source size				Mechanism plane A [deg]			Mechanism plane B [deg]		
Year	Data	Time	X [m]	Y [m]	Z [m]	M	E [J]	M ₀ [N-m]	r[m]	Strike	Dip	Rake	Strike	Dip	Rake
1994	31-Aug	20:33	34850	5633	-890	3.4	7.3E+07	9.4E+13	267	213	55	78	54	36	107
1994	1-Sep	21:27	34386	5532	-870	3.0	1.2E+07	3.7E+13	228	240	66	116	9	34	45
1994	2-Sep	21:19	33033	8497	-910	3.1	1.5E+07	3.4E+13	231	139	54	99	304	37	78
1994	14-Oct	18:17	32904	4480	-750	3.0	1.1E+07	1.0E+13	171	188	89	108	282	18	4
1994	18-Oct	11:12	33432	8817	-940	3.3	4.2E+07	5.2E+13	185	196	77	77	61	19	134
1994	22-Nov	13:29	28512	7028	-740	3.4	7.3E+07	4.6E+13	277	114	85	-86	255	6	-129
1994	5-Dec	23:45	28354	7053	-740	3.1	1.4E+07	3.3E+13	265	138	88	-91	351	2	-57
1994	10-Dec	14:35	32687	4778	-760	3.3	3.9E+07	1.0E+14	306	33	82	73	278	18	154
1994	21-Dec	13:26	27203	9390	-690	3.6	2.0E+08	2.9E+14	502	348	62	-99	187	28	-73
1994	22-Dec	9:23	27419	9023	-680	3.0	1.1E+07	1.4E+13	178	12	61	-80	171	31	-108
1995	31-Mar	2:57	27680	7622	-550	3.1	9.5E+07	4.4E+13	202	140	87	-87	272	8	-138
1995	26-May	4:57	33500	8600	-1050	3.8	2.9E+08	5.6E+14	416	140	41	-92	323	49	-89
1995	24-Aug	16:46	34986	5601	-800	3.3	3.6E+07	9.1E+13	280	318	74	-119	202	33	-31
1995	14-Sep	19:39	32699	4699	-470	3.2	3.1E+07	3.3E+13	167	17	87	140	109	50	3
1995	1-Oct	13:06	32818	4298	-900	3.0	8.8E+06	1.7E+13	186	63	57	86	251	34	96
1995	10-Oct	18:17	33352	8678	-920	3.0	9.6E+06	1.9E+13	230	309	89	-95	209	5	-11
1995	23-Nov	6:03	28452	6952	-740	3.6	1.4E+08	7.6E+13	280	123	54	-82	290	37	-100
1995	2-Dec	10:13	34493	5812	-650	3.0	1.1E+07	2.5E+13	301	179	46	-88	356	44	-92
1997	11-Mar	20:13	31569	5947	-700	3.1	2.0E+07	1.6E+14	467	130	47	97	299	43	82
1997	17-Apr	12:35	31656	10539	-775	3.4	6.0E+07	1.6E+14	445	356	69	-48	107	46	-151
1997	26-Apr	10:52	31640	9885	-1025	3.0	1.2E+07	5.5E+13	305	0	88	-64	94	26	-175
1997	26-Apr	14:23	31233	6155	-975	3.2	2.9E+07	7.3E+13	348	133	72	-80	283	20	-119
1997	29-Apr	17:11	30826	6060	-900	3.2	2.8E+07	3.7E+13	275	233	47	89	54	43	91
1997	13-Jun	15:22	31624	6007	-1050	3.1	2.1E+07	9.6E+13	374	101	64	36	353	58	149
1997	28-Jun	21:50	31229	6201	-725	3.4	6.9E+07	1.1E+14	387	360	52	76	202	41	107
1997	3-Jul	22:00	31618	10542	-950	3.1	1.5E+07	1.1E+14	428	335	79	-83	124	13	-120
1997	23-Jul	23:49	31674	7112	-800	3.1	1.4E+07	4.8E+13	245	103	88	174	193	84	2
1997	30-Aug	16:43	30432	6067	-825	3.0	1.1E+07	4.7E+13	252	271	64	-121	145	40	-44
1998	31-Jul	16:22	31223	5928	-750	3.0	8.8E+06	4.1E+13	284	97	62	84	288	29	100
1998	31-Jul	18:51	30449	6147	-750	3.3	4.5E+07	6.1E+13	279	78	87	75	336	15	167
1998	28-Aug	14:59	28792	6805	-720	3.0	1.1E+07	5.6E+12	202	223	84	111	327	22	15
1998	31-Aug	5:40	31252	9910	-900	3.2	3.0E+07	9.1E+13	378	210	77	98	357	15	58
1998	10-Sep	5:03	32473	8882	-930	3.4	5.5E+07	6.0E+13	325	99	67	94	270	23	81
1998	22-Sep	21:56	27591	8608	-750	3.3	3.5E+07	2.6E+13	331	44	47	85	231	43	95
1998	3-Oct	15:49	32977	8808	-860	3.2	2.7E+07	2.9E+13	215	110	85	-92	312	5	-68
1998	20-Oct	2:07	27472	8510	-750	3.1	1.9E+07	3.9E+13	346	198	68	93	10	23	83
1998	5-Nov	10:23	32686	4663	-600	3.0	8.6E+06	2.3E+13	265	120	76	83	325	16	114
1998	6-Nov	13:13	30112	6167	-770	3.5	1.1E+08	6.9E+13	337	91	66	100	249	26	70
1998	28-Nov	21:18	32375	8892	-920	3.3	5.0E+07	5.5E+13	314	330	68	44	220	50	150
1998	10-Dec	0:20	28209	6173	-690	3.2	3.0E+07	4.5E+13	318	88	57	56	319	46	131
1999	18-Jul	5:45	31165	9966	-810	4.2	2.0E+09	5.1E+14	582	192	88	89	39	3	117
1999	27-Jul	16:30	29088	7448	-900	3.2	2.8E+07	5.1E+13	279	170	66	99	328	26	70
1999	12-Aug	1:37	31000	6109	-750	3.1	1.9E+07	3.7E+13	241	359	88	93	125	4	36
1999	23-Aug	3:20	27428	8375	-700	3.6	1.5E+08	7.5E+13	360	30	77	-51	135	40	-160

Table 3

Origin			Source size			Slip [cm]			Origin			Source size			Slip [cm]		
Year	Data	Time	r[m]	L[m]	W[m]	u	ss	sd	Year	Data	Time	r[m]	L[m]	W[m]	u	ss	sd
1994	31-Aug	20:33	267	580	386	1.91	-0.40	1.87	1997	29-Apr	17:11	275	598	398	0.70	-0.02	0.70
1994	1-Sep	21:27	228	495	330	1.03	0.45	0.93	1997	13-Jun	15:22	374	812	541	1.00	-0.81	0.59
1994	2-Sep	21:19	231	501	334	0.92	0.14	0.91	1997	28-Jun	21:50	387	841	560	1.06	-0.26	1.03
1994	14-Oct	18:17	171	371	247	0.50	0.16	0.47	1997	3-Jul	22:00	428	928	619	0.90	-0.11	-0.90
1994	18-Oct	11:12	185	402	268	2.20	-0.51	2.14	1997	23-Jul	23:49	245	532	354	1.16	1.15	0.12
1994	22-Nov	13:29	277	601	401	0.87	-0.06	-0.87	1997	30-Aug	16:43	252	546	364	1.07	0.55	-0.91
1994	5-Dec	23:45	265	575	384	0.68	0.01	-0.68	1998	31-Jul	16:22	284	616	410	0.73	-0.07	0.73
1994	10-Dec	14:35	306	664	443	1.55	1.39	0.67	1998	31-Jul	18:51	279	605	403	1.14	-0.29	1.10
1994	21-Dec	13:26	502	1090	727	1.67	0.27	-1.64	1998	28-Aug	14:59	202	437	292	0.20	0.07	0.19
1994	22-Dec	9:23	178	386	258	0.64	0.19	-0.61	1998	31-Aug	5:40	378	821	547	0.92	0.13	0.91
1995	31-Mar	2:57	202	439	292	1.56	-0.10	-1.55	1998	10-Sep	5:03	325	706	470	0.82	0.05	0.82
1995	26-May	4:57	416	903	602	4.69	0.14	-4.69	1998	22-Sep	21:56	331	719	479	0.34	-0.03	0.34
1995	24-Aug	16:46	280	608	405	1.68	0.82	-1.47	1998	3-Oct	15:49	215	467	311	0.90	0.03	-0.90
1995	14-Sep	19:39	167	363	242	1.71	1.32	1.09	1998	20-Oct	2:07	346	750	500	0.48	0.03	0.47
1995	1-Oct	13:06	186	404	269	0.71	-0.05	0.71	1998	5-Nov	10:23	265	575	383	0.48	-0.06	0.47
1995	10-Oct	18:17	230	499	333	0.52	0.04	-0.52	1998	6-Nov	13:13	337	732	488	0.87	0.15	0.86
1995	23-Nov	6:03	280	608	405	1.40	-0.19	-1.39	1998	28-Nov	21:18	314	681	454	0.81	-0.58	0.57
1995	2-Dec	10:13	301	653	436	0.40	-0.01	-0.40	1998	10-Dec	0:20	318	690	460	0.65	-0.36	0.54
1997	11-Mar	20:13	467	1013	675	1.07	0.14	1.06	1999	18-Jul	5:45	582	1263	842	2.18	-0.04	2.18
1997	17-Apr	12:35	445	966	644	1.19	-0.80	-0.88	1999	27-Jul	16:30	279	606	404	0.95	0.16	0.94
1997	26-Apr	10:52	305	662	441	0.85	-0.37	-0.76	1999	12-Aug	1:37	241	523	349	0.92	0.05	0.92
1997	26-Apr	14:23	348	756	504	0.88	-0.16	-0.86	1999	23-Aug	3:20	360	781	521	0.84	-0.52	-0.65

Figure 1. Spatial distribution of the analyzed events with $2.0 < M_L < 2.9$ (gray small circles) and $M_L > 3.0$ (black circles) along with the seismic stations (triangles). The dashed rectangle outlines the area of study shown in Figure 4.

Figure 2. Histograms of a. the isotropic component ISO, b. the linear vector dipole component CLVD and c. the double couple component DC in the total moment tensor solutions of the analyzed seismic events of the Rudna Coal Mine.

Figure 3. Histogram of the frequency of the occurrence of seismic events of a. magnitude $M_L \geq 2.0$ and b. seismic moment $M_0 \geq 10^{13}$ [N·m], that occurred during 06.1993 – 08.1999 in the Rudna Mine area in the Legnica–Głogów Copper District as a function of ΔCFF .

Figure 4. Accumulated stress changes in the G-1/7 field of the Rudna Mine in LGCD, the west part of Poland from 06.06.1993 to 13.08.1999. Coulomb stress is calculated for faults at a depth of 0.9 km. The stress pattern is calculated for the faulting type of the next mine event in the data sample. Changes are denoted by a color scale shown in the right part of each figure (in bars). The Coulomb failure function (CFF) is taken to be equal to the state of stress after the first 76 tremors that occurred between 06.06.1993 and 23.04.1996. The green line denotes the fault trace projected up-dip at the Earth's surface, the black one is the intersection of target depth with fault plane, the grey rectangle is the frame of the fault projected to the surface. a. coseismic Coulomb stress changes before 23.04.1996, the stress field is inverting according to the fault plane solution of the 23.04.1996 event; b. stress evolution until just before the 07.11.1996 event; c. the state of stress just before the occurrence of the 08.11.1996 tremor; d. cumulative stress changes until just before the 19.12.1996 event; e. the state of CFF before the event on 09.09.1998; f. cumulative stress changes before the event occurred on 13.10.1998; g. the stress pattern just before the 04.07.1999 tremor; h. the state of stress before the 05.07.1999 event; i. stress evolution just up to the event occurred on the 12.08.1999; j. the stress field before the occurrence of the 13.08.1999 event.

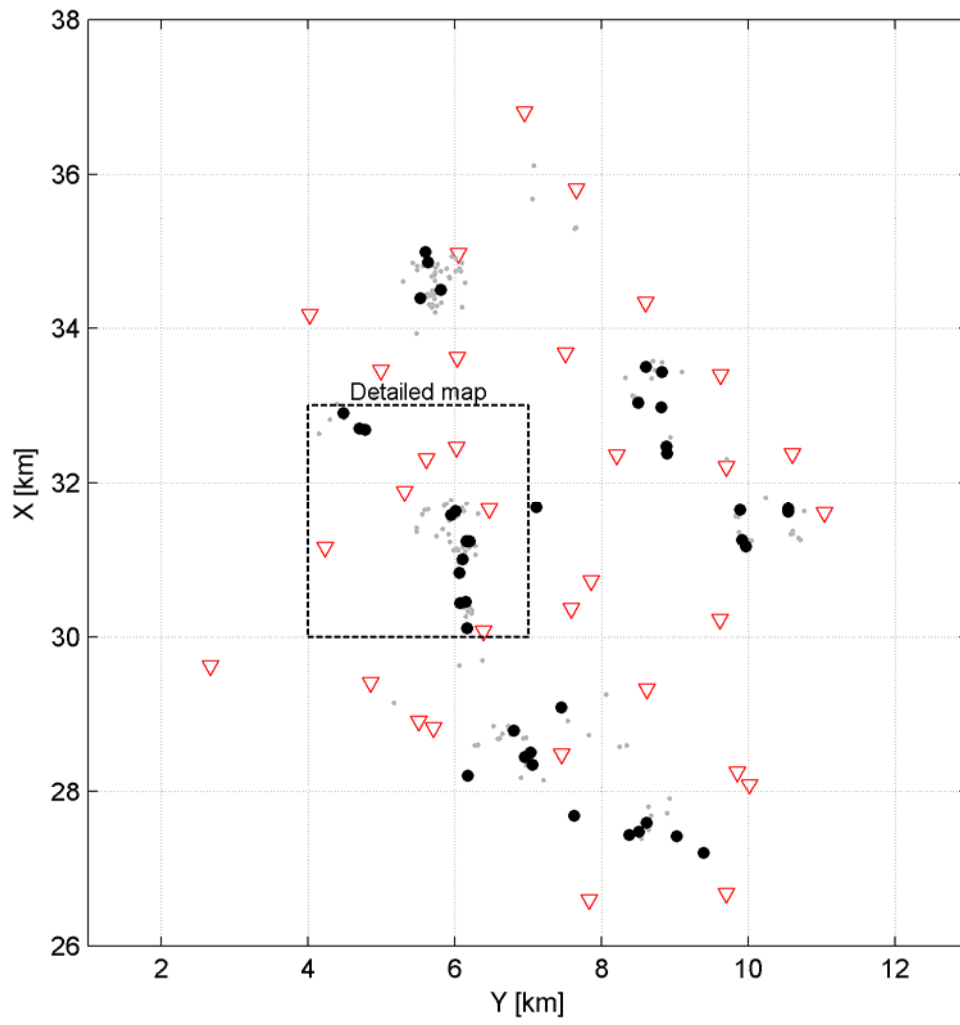
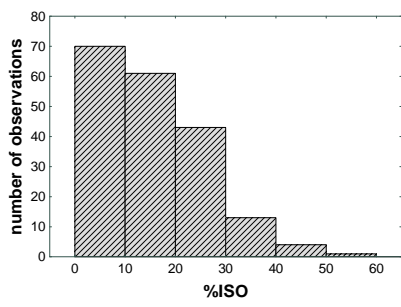
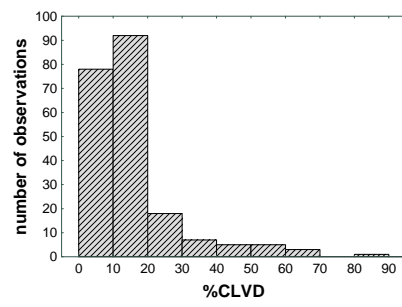


Figure 1.

a.



b.



c.

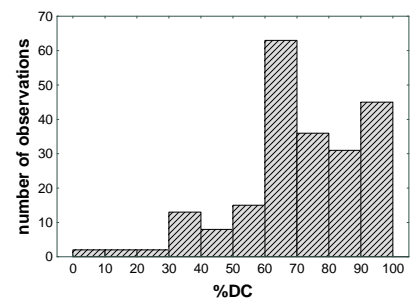
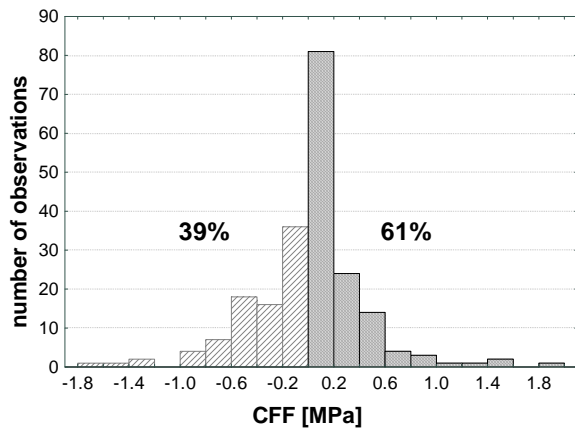


Figure 2.

a.



b.

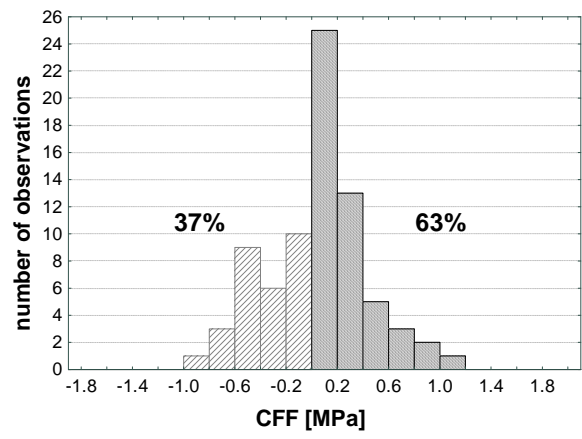
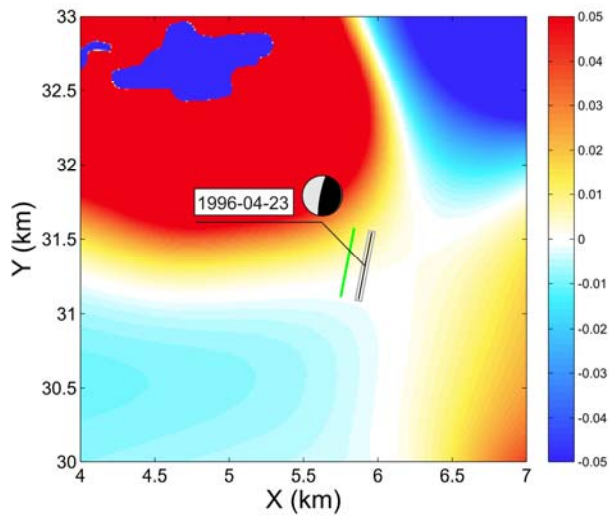
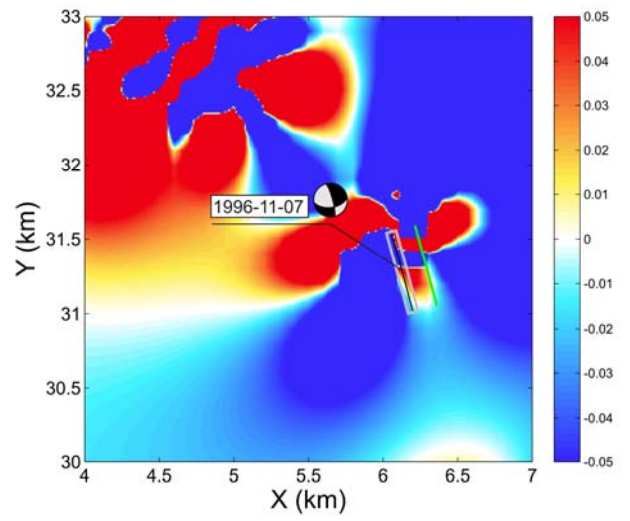


Figure 3.

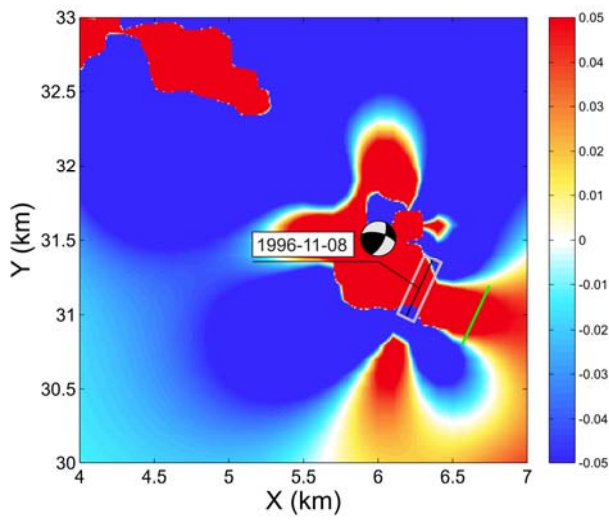
a.



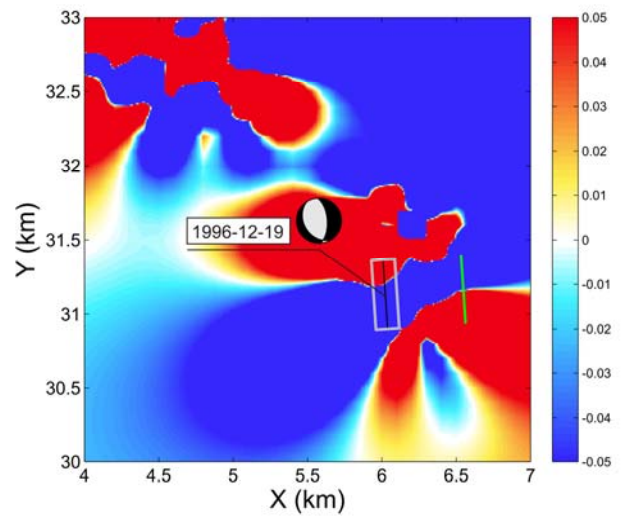
b.



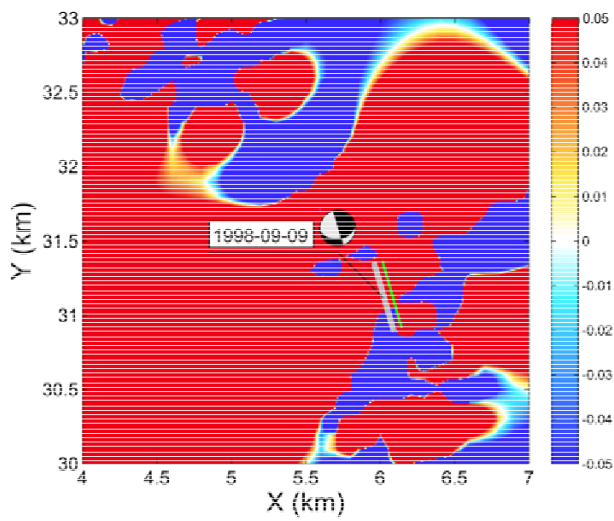
c.



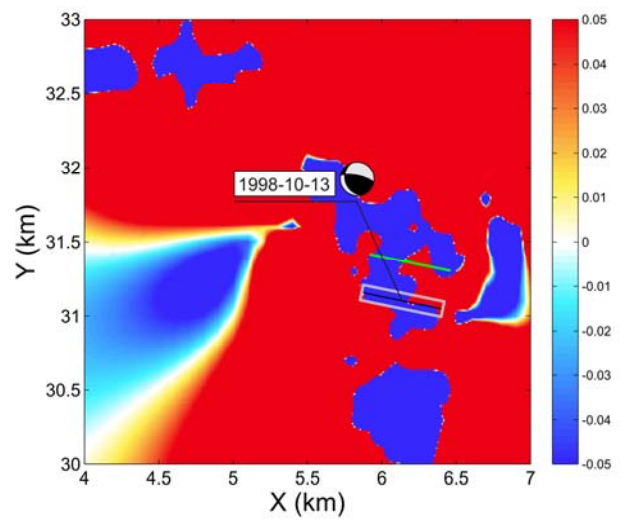
d.



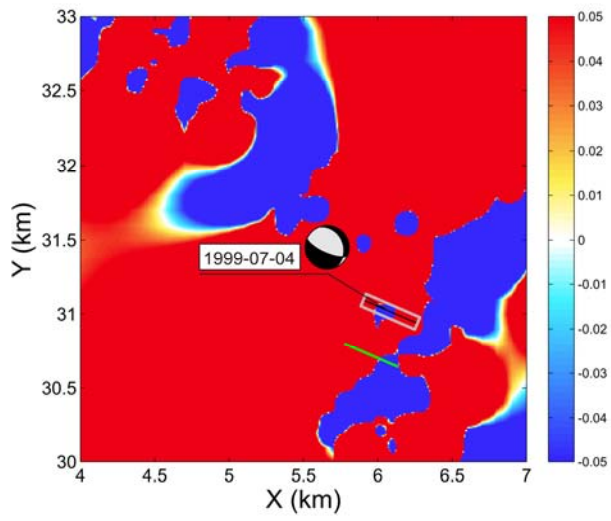
e.



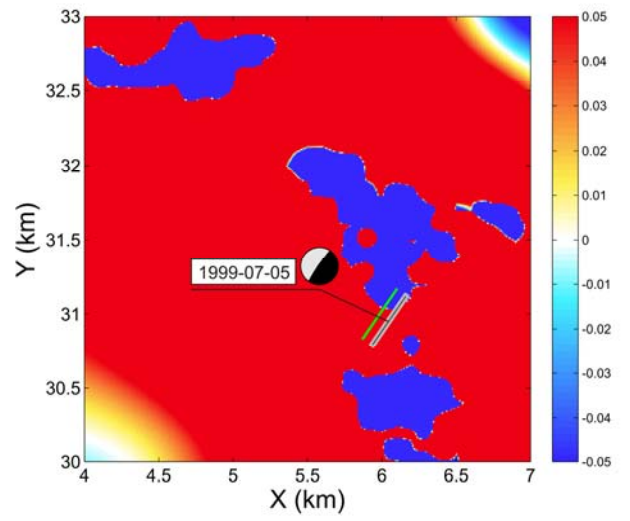
f.



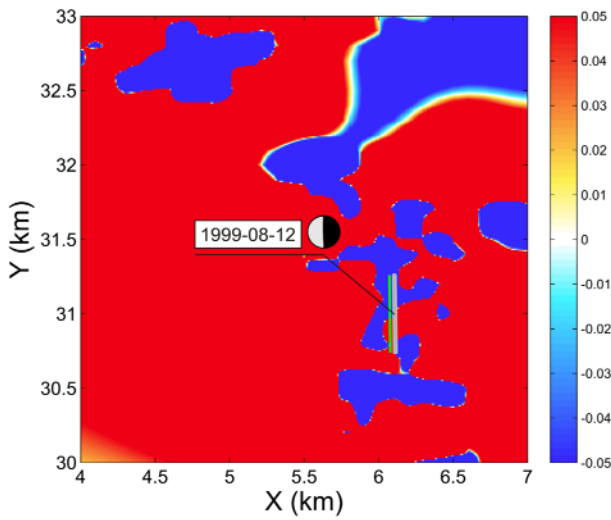
g.



h.



i.



j.

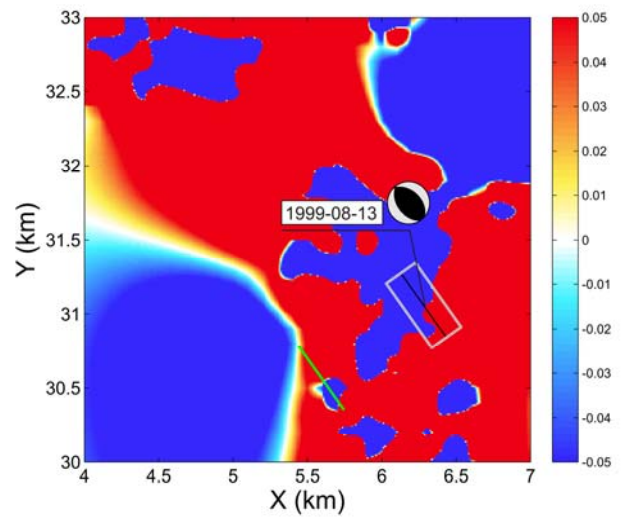


Figure 4.